DOI 10.1007/s11141-021-10097-5
Radiophysics and Quantum Electronics, Vol. 63, Nos. 9–10, February–March, 2021
(Russian Original Vol. 63, Nos. 9–10, September–October, 2020)

LOSS OF STABILITY OF THE BLOOD LIQUID STATE AND ASSESSMENT OF SHEAR-INDUCED THROMBOSIS RISK

D. M. Pushin,[1,2*] **T. Yu. Salikhova,**[1,2]
L. S. Biryukova,[1] **and G. Th. Guria** [1,2]

UDC 51-76+577.359

The loss of stability of the blood liquid state causes changes in the blood aggregation, resulting in thrombus formation. Intravascular thrombus formation is intensely studied within modern biophysics by the methods of mathematical simulation. Determining the conditions of shear-induced platelet activation has opened an opportunity for the estimation of thrombus formation risks in particular clinical settings. In this paper, a new approach is proposed to determine the risks of shear-induced thrombus formation. This approach is applicable for a wide range of objects including aorta and mechanical circulatory assist devices. The geometry of the vascular walls in numerical experiments is chosen to be isomorphic to that of the blood vessels in a human body. Promising ways to reduce the risks of thrombus formation activation in high blood flows have been found. The developed technique can be used by physicians to plan personalized strategies for antithrombotic therapy based on individual shear-induced platelet activation risks.

1. INTRODUCTION

Methods of nonlinear dynamics are intensely used to determine the conditions of destabilization of vital regulation systems of the human body [1, 2]. One of such systems is the blood coagulation system, the disorder of which leads to the development of serious thrombotic complications. Analysis of the blood liquid state stability shows that the conditions for initiating intravascular blood coagulation depend significantly on the blood flow pattern [3, 4].

In low blood flows (in venules, arterioles, and capillaries), the blood coagulation is usually initiated by damaging the vascular wall. In high flows (in large arteries), intravascular coagulation can be enabled by the flow itself without violating the vessel integrity [5, 6]. Thrombus formation activation in large arteries is of great clinical interest due to the risk of complications that it can lead to (heart attacks and strokes). Despite the considerable progress in studying the conditions of thrombus formation activation in high blood flows, the direct application of the scientific results to the analysis of clinical risks cannot be properly implemented without taking the features of hemodynamics in the thrombogenically dangerous part of the circulatory system into account.

The features of the blood flow in a large vessel depend significantly on its geometric characteristics, such as diameter, curvature, and the presence or absence of vascular wall pathologies. It was only possible to speculate about the shear-induced effect on the intravascular thrombus formation processes [7, 8] before the advent of methods for effective imaging of anatomical structures.

* pushin@phystech.edu

[1] National Medical Research Center of Hematology, Moscow; [2] Moscow Institute of Physics and Technology, Dolgoprudny, Russia. Translated from Izvestiya Vysshikh Uchebnykh Zavedenii, Radiofizika, Vol. 63, Nos. 9–10, pp. 894–918, September–October 2020. Original article submitted June 14, 2020; accepted October 28, 2020.

However, due to the development of radiocontrast angiography, as well as optical, acoustic, and magnetic resonance spectroscopy methods in the XXth century, it became possible to perform a detailed visualization of biological structures [9–11]. This enabled the physicians to judge the anatomical features of the vessels. The advent of dynamic methods that record variations in the time of processes in organs and tissues, in particular, made it possible to detect the state of hemodynamics in bodies of particular patients in real time [12–14].

The extension of the list of tools for monitoring of blood hemodynamics, on the one hand, and the development of methods for mathematical simulation of blood coagulation activation processes, on the other hand, have opened up a fundamental opportunity for assessment of intravascular thrombus formation risks with allowance for realistic blood flow features in potentially thrombogenic vessels. In this paper, these methods are employed to determine the shear-induced activation risks in vessels that are isomorphic in their geometry to those present in the body, and also in mechanical circulatory assist devices used to maintain hemodynamics. The obtained results can be exploited by physicians to plan strategies for antithrombotic therapy with allowance for shear-induced platelet activation risks.

2. MODERN CONCEPTS OF SHEAR-INDUCED ACTIVATION OF THROMBUS FORMATION

2.1. Shear stress and methods of its calculation

Methods of computational fluid dynamics (CFD) are widely used to describe hemodynamics in a human body [15, 16]. Modern CFD methods are used to find spatiotemporal distributions of biomechanical characteristics, in particular, shear stress [17]. The calculation of the shear stress distribution is routine for large human vessels, whose anatomical features are recovered by processing of images obtained by radiodiagnosis (computed tomography, magnetic resonance imaging, and ultrasound research) [18, 19].

Blood in large vessels can be considered a Newtonian fluid, i. e., a fluid with a viscosity independent of the shear rate [20]. In biomechanics, shear stress is most often referred to as a wall shear stress [20–22]. Within the physiological norm, the shear stress, generally speaking, is not the same in different parts of the cardiovascular system [23]. Thus, the shear stress ranges from 10 to 30 dyn/cm^2 in non-stenotic arteries with a diameter of more than 2 mm (this corresponds to a shear rate of $250\,\mathrm{s}^{-1} < \dot{\gamma} < 750\,\mathrm{s}^{-1}$). In a number of smaller arteries, the shear stress normally reaches 60 dyn/cm^2 ($\dot{\gamma} = 1500\,\mathrm{s}^{-1}$) [24, 25]. In pathological conditions, e. g., in the development of atherosclerotic disease of large vessels, the shear stress can exceed 1000 dyn/cm^2 [26]. A number of authors point out that dynamic variations in the shear stress can serve as a factor that regulates the vascular tone, causing a change in the diameter of the vessels [27].

The shear stress is considered a key mechanical characteristic of the blood flow that affects the shear-induced activation of thrombus formation [28, 29]. High shear stresses can initiate the thrombus formation process due to direct mechanical damage of platelets, accompanied by their activation in the bloodstream, and due also to injury of endothelial cells lining the inner surface of the vessel [30, 31]. In the latter case, platelets are attached to the site of injury due to specific receptors on their surface, which causes their further activation.

The simplest estimate of the shear stress in a vessel is based on the assumption of a Poiseuille velocity profile: $\tau = 32\eta Q/(\pi d^3)$, where η is the blood viscosity, Q is the volume flow, and d is the vessel diameter. This technique is commonly used in the Doppler ultrasound data interpretation [32].

At present, another method for the shear stress finding in large human vessels, based on four-dimensional flow magnetic resonance imaging (4D Flow MRI), is being intensely developed [33]. This method provides a high spatial and temporal resolution for recovery of the shear rate/stress distribution within the cardiac cycle over the entire study area of the blood flow.

2.2. The shear stress effect on the hemostatic system activation

A comparison of the CFD and 4D Flow MRI methods shows that both approaches explicitly or implicitly use ideas concerning the rheological blood properties in the shear stress assessment [17, 36, 37].

However, blood by its nature cannot be classified as a liquid with a certain rheology. When blood changes its aggregate state, the nature of the relation between the stress tensor and the strain rate tensor cannot be specified algebraically [4].

The fact is that blood within the physiological norm is a metastable substance that can, under certain external chemical and hydrodynamic impacts, experience a transition with a change in the aggregate state [3, 38]. During the last quarter of the century, attempts to develop physical and mathematical models that are able to study blood coagulation under low hemodynamic conditions (with the Reynolds number $\mathrm{Re} \ll 1$) have been made [39–41].

Within the framework of such approaches, along with the hydrodynamic characteristics (velocity and pressure fields), the biochemical factors of blood coagulation and, in certain cases, the formed elements of blood (platelets and erythrocytes) involved in the thrombus formation processes were taken into account [42–46]. In particular, it was shown how activation of the blood coagulation system is able to provoke thrombus formation in stagnant zones distal to the stenotic site.

If the blood vessel wall is not damaged, then the plasma factor of the blood coagulation is not activated. The blood remains in a liquid state. In the presence of damage, the threshold for blood coagulation activation decreases as the blood flow slows down [40]. As a result, the thrombus formation risk increases. In such cases, thrombus formation can be initiated when the pressure in the vessel is below the critical level. Further, the conclusion about the effect of slowing blood flow on lowering the threshold of blood coagulation activation was confirmed experimentally [47]. The result concerns the activation of coagulation in small vessels, particularly in venules.

It is known that not only a sharp drop in blood pressure, but also hypertension oscillations can provoke the intravascular blood coagulation activation in some cases [48, 49]. In particular, an increase in blood pressure (and, as a result, tangential shear stresses in the blood flow) leads to an increase in permeability of the vascular walls for primary procoagulants [4]. In this case, plasma hemostasis activation occurs due to a violation of the integrity of the endothelial layer of the vascular walls in the range of shear rates $250\,\mathrm{s}^{-1} < \dot{\gamma} < 1000\,\mathrm{s}^{-1}$ ($10\,\mathrm{dyn/cm}^2 < \tau < 40\,\mathrm{dyn/cm}^2$) [4]. It is worth noting that shear-induced platelet activation does not take place in this range of shear rates.

In some situations, the shear stresses may exceed the range of values mentioned above. For shear stresses above 200 $\mathrm{dyn/cm}^2$ ($\dot{\gamma} > 5400\,\mathrm{s}^{-1}$), platelet activation can be provoked with the subsequent participation of platelets in the formation of blood clots in the vessels [5, 50, 51]. It should be noted that platelet activation in large arteries is almost absent within the physiological norm [28, 29]. Conditions for shear-induced platelet activation can develop in a number of vascular pathologies (aneurysms, malformations, and atherosclerotic plaques).

Concepts concerning the existence of the shear stress threshold value (shear rate) were formed as a result of *in vitro* experiments. *In vitro* systems use cone–plate viscometers to study the shear activation and platelet aggregation. Devices of this type create flow regions with uniform shear stresses [28]. Blood or a platelet-rich plasma is used in the experiments and is exposed to increased shear stresses ($\tau > 50\,\mathrm{dyn/cm}^2$) for a few minutes [31]. The result of experiments, as a rule, is the dependence of the platelet activation level on the shear stress.

In a human body, blood circulates in the cardiovascular system, in different parts of which, generally speaking, the shear stresses are not the same. As a result, the thrombus activation is primarily initiated in the vessels in which the shear stress exceeds the critical level τ_c: $\tau > \tau_c$. At the same time, the value of the critical shear stress τ_c itself, despite the numerous experiments, remains controversial. According to a number of *in vitro* studies, its value ranges from 40 to 400 $\mathrm{dyn/cm}^2$ [52–55].

The question of what biophysical and biochemical factors can determine the τ_c value is intensely discussed in the literature [5, 56–58]. A number of papers show that the von Willebrand factor (VWF) macromolecules play a key role in the platelet shift activation [59, 60]. These molecules are macromolecular complexes, normally consisting of 2–80 subunits [61, 62]. Each subunit acting as a monomer has a domain structure. One of the domains, A1, is able to bind to GPIb receptors located on the surface of platelets.

Multivalent binding of VWF molecules to GPIb complexes on a separate platelet may initiate its activation, leading to a subsequent aggregation [63, 64].

Hydrodynamic conditions regulate the binding of VWF to platelets by changing the conformation of VWF multimers in shear flows [65]. At low shear stresses in the blood flow, VWF multimers have a compact globular conformation, in which only a small number of A1 domains are available for binding to platelets [60, 66–68]. When the shear stress increases above the critical value, the VWF molecules unfold, increasing the number of A1 domains exposed on the surface [61, 69, 70]. It was shown that platelet activation due to the VWF occurs only at supercritical shear stresses [31, 52, 53, 71]. Moreover, the length of the VWF molecules correlates with the platelet activation and aggregation levels [72–74]. This gave grounds to suppose that the τ_c value depends on the size of the VWF molecules [56, 75].

This hypothesis has been analyzed in a recent paper [5]. Its authors constructed a bifurcation diagram of states that shows the unwinding degree of VWF molecules on the platelet surface as a functon of the shear stress (see Fig. 1). The diagram demonstrates the existence of two bifurcation values of the shear stress. When the shear stress exceeds the smaller value (τ_*), the VWF molecules start to unwind, and the molecule goes into a fully unwound stable state when the second value (τ_c) is exceeded.

The authors have obtained a condition for platelet activation in the form

$$\tau > \tau_{\rm cr}, \tag{1}$$

where τ is the shear stress acting on the VWF molecules on the platelet surface, and $\tau_{\rm cr}$ is the critical shear stress, which depends on the degree n of multimericity of VWF molecules as follows:

$$\tau_{\rm cr} = 3 \cdot (3/2)^{4/3} \tau_c \frac{(n - n_{\rm a})^{1/3} - (2/3)^{1/3}}{n - n_{\rm a}}. \tag{2}$$

Here, $n_{\rm a}$ is the minimum length of the VWF molecule "tail" required for the platelet activation.

Analysis of conditions (1) and (2) shows that platelet activation can occur in shear flows of sufficient intensity. The critical shear stress $\tau_{\rm cr}$ can be regulated by varying the VWF multimericity degree.

The actual shear stress τ in the blood flow is determined by the amount of cardiac output, blood pressure, stenosis degree, and other hemodynamic vessel characteristics. Thus, Eqs. (1) and (2) show that the intravascular thrombus formation risks can be controlled both by correcting systemic hemodynamic parameters (e. g., by changing blood pressure, using statins, etc.) and by controlling the distribution of VWF molecules by their multimericity degree (due to ADAMTS-13 metalloproteinase).

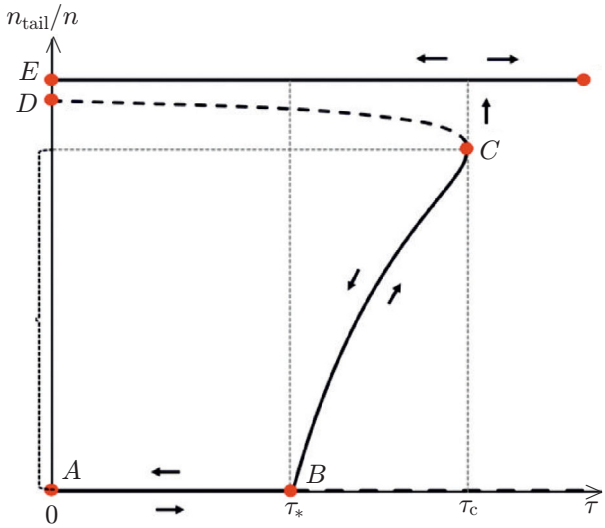

Fig. 1. Bifurcation diagram of the conformational stability of VWF molecules at different shear stresses. Solid bold lines represent branches corresponding to stable stationary states, dashed lines represent unstable stationary states, τ_* is the bifurcation value of the shear stress, $\tau_{\rm c}$ is the shear stress at which the VWF molecule must be completely unwound. The degree of VWF unwinding on the platelet surface was defined as the ratio of the number $n_{\rm tail}$ of monomeric subunits in the unwound part of the VWF molecule to the total number n of such subunits in it. The point A corresponds to the globular state, E, to the fully unwound state, and the brace, to the regions of partially unwound states. Adapted from [5].

Note that the above results were obtained in the approximation of a quasi-static change in the shear stress. This approximation is correct for *in vitro* situations (e. g., in experiments with the use of torsion viscometers), as well as near the vessel walls or implantable devices.

The mechanism of platelet activation in nonstationary pulse flows has been considered in a recent paper [76]. It developed an approach to the study of critical conditions of the shear-induced platelet activation based on the concepts of the cumulative shear-stress role.

3. METHODS FOR ASSESSMEMT OF SHEAR-INDUCED INTRAVASCULAR THROMBUS FORMATION RISKS

The level of the shear-induced platelet activation is insignificant in the physiological norm [59]. Areas of increased shear stresses may develop in large vessels with pathologies or in devices for maintaining blood circulation. The penetration of platelets into these areas, even for a short time, can lead to their activation [76].

The approach to assessing the shear-induced platelet activation risks used in this study was based on the results of [5]. It was assumed that platelet activation occurs in a threshold manner, when the shear stress exceeds the critical value (see Eqs. (1) and (2)).

The shear stress τ in Eq. (1) was calculated as follows. At the first stage, the fields of the velocity $\mathbf{V}(x, y, z, t)$ and the pressure $p(x, y, z, t)$ were determined by numerically solving the Navier–Stokes equations in the form

$$\frac{\partial \mathbf{V}}{\partial t} + (\mathbf{V}, \nabla)\,\mathbf{V} = -\frac{1}{\rho}\nabla p + \nu \Delta \mathbf{V}, \tag{3}$$

$$(\nabla, \mathbf{V}) = 0, \tag{4}$$

where t is the time, x, y, and z are the Cartesian coordinates, ∇ is the Hamilton operator, ρ is the density, ν is the kinematic blood viscosity, and Δ is the Laplace operator. The Poiseuille velocity profile was specified as a boundary condition at the input cross section, and the zero pressure condition was set at the output cross section. The impermeability and non-slip condition was assumed to be fulfilled on the walls [77].

Further, the shear rate $\dot{\gamma}$ was calculated from the found velocity field [78]:

$$\dot{\gamma} = \sqrt{2}\sqrt{\left(\frac{\partial V_x}{\partial x}\right)^2 + \left(\frac{\partial V_y}{\partial y}\right)^2 + \left(\frac{\partial V_z}{\partial z}\right)^2 + \frac{1}{2}\left(\frac{\partial V_x}{\partial y} + \frac{\partial V_y}{\partial x}\right)^2 + \frac{1}{2}\left(\frac{\partial V_x}{\partial z} + \frac{\partial V_z}{\partial x}\right)^2 + \frac{1}{2}\left(\frac{\partial V_y}{\partial z} + \frac{\partial V_z}{\partial y}\right)^2}. \tag{5}$$

Here, V_x, V_y, and V_z are the velocity-vector components. In this case, the absolute value of the shear stress τ was specified by the expression

$$\tau = \eta \dot{\gamma}, \tag{6}$$

where η is the dynamic blood viscosity. The distributions of the concentrations of the activated and inactivated platelets in the blood flow during their interaction with VWF molecules having the specified multimericity degree n were found by solving the system of equations

$$\frac{\partial P}{\partial t} + (\mathbf{V}, \nabla)\,P = -kP\theta(\tau - \tau_{\mathrm{cr}}), \tag{7}$$

$$\frac{\partial P_{\mathrm{a}}}{\partial t} + (\mathbf{V}, \nabla)\,P_{\mathrm{a}} = kP\theta(\tau - \tau_{\mathrm{cr}}), \tag{8}$$

where P is the concentration of inactivated platelets, P_{a} is the concentration of activated platelets, k is the rate constant of the platelet transition from inactivated to activated state, $\theta(\tau - \tau_{\mathrm{cr}})$ is the Heaviside function, and the τ_{cr} value for each particular n was determined by Eq. (2).

At the input cross section of the vessel, the concentration of inactivated platelets was assumed to be constant and equal to the physiological value, whereas the concentration of activated platelets was considered to be zero. At the output cross section of the considered vascular configuration, the condition of a zero gradient of non-activated and activated platelets was set.

The platelet activation degree was characterized by the platelet activation index (PAI):

$$\mathrm{PAI} = \left[\frac{1}{\Delta t}\int\limits_{t_0}^{t_0+\Delta t} (J_{\mathrm{a}}/J_{\Sigma})\,\mathrm{d}t\right] \cdot 100\%, \tag{9}$$

where Δt is the cardiac cycle duration, t_0 is the start time of the cardiac beat, during which the averaging was performed, and J_a and J_Σ are the convective flow of activated platelets and the total convective flow of platelets through the output cross section Γ_out, respectively:

$$J_\mathrm{a} = \int\limits_{\Gamma_\mathrm{out}} P_\mathrm{a}\mathbf{V}\,\mathrm{d}\mathbf{S}, \tag{10}$$

$$J_\Sigma = \int\limits_{\Gamma_\mathrm{out}} (P + P_\mathrm{a})\mathbf{V}\,\mathrm{d}\mathbf{S}. \tag{11}$$

The symbol $\mathrm{d}\mathbf{S}$ indicates an element of the output cross-sectional area.

The risk of platelet activation in turbulent flows was assessed on the basis of the Reynolds averaged Navier–Stokes (RANS) equations, which are formally reduced to taking into account the turbulent kinematic viscosity ν_t in the equations of motion [79, 80]:

$$\frac{\partial \mathbf{V}}{\partial t} + (\mathbf{V}, \nabla)\,\mathbf{V} = -\frac{1}{\rho}\nabla p + (\nu + \nu_t)\Delta\mathbf{V}, \tag{12}$$

$$(\nabla, \mathbf{V}) = 0. \tag{13}$$

The $k-\omega-$SST turbulence model was used to calculate ν_t [81].

The calculated field of turbulent kinematic viscosity ν_t was further used to calculate the distributions of inactivated and activated platelets:

$$\frac{\partial P}{\partial t} + (\mathbf{V}, \nabla)\,P = D_t\Delta P - kP\theta(\tau - \tau_\mathrm{cr}), \tag{14}$$

$$\frac{\partial P_\mathrm{a}}{\partial t} + (\mathbf{V}, \nabla)\,P_\mathrm{a} = D_t\Delta P_\mathrm{a} + kP\theta(\tau - \tau_\mathrm{cr}). \tag{15}$$

Here, $D_t = \nu_t/\mathrm{Sc}$ is the turbulent diffusion coefficient [79], Sc is the Schmidt number, and the absolute value of the shear stress was determined by the expression

$$\tau = (\eta + \eta_t)\dot{\gamma}. \tag{16}$$

It was assumed throughout that the equality $\eta_t = \rho\nu_t$ takes place. The degree of platelet activation was determined by Eq. (9).

For information on the programs and numerical methods used to analyze the platelet activation risk, see Appendices 1 and 2. The ranges of parameter values used in the numerical calculations are given in Table P1.1 of Appendix 1.

The developed approach was employed by the authors of this paper to create a software and hardware system for assessment of thrombus formation risks (Russian Science Foundation project Nos. 19-11-00260 and 14-14-00990). This software and hardware system is designed to solve problems of clinical interest.

4. ASSESSMENT OF SHEAR-INDUCED THROMBUS FORMATION RISKS

4.1. Assessment of shear-induced platelet activation risks in large vessels

This paper analyzes the risk of shear-induced thrombus formation in the aorta having a pronounced narrowing of the lumen (stenosis). This narrowing is detected by magnetic resonance angiography (see Fig. 2). In the region of greatest narrowing, supercritical shear stresses may occur. The magnitude of the critical shear stresses is determined by the multimericity of the VWF molecules. The degree of platelet activation was assessed based on the method described in Sec. 3.

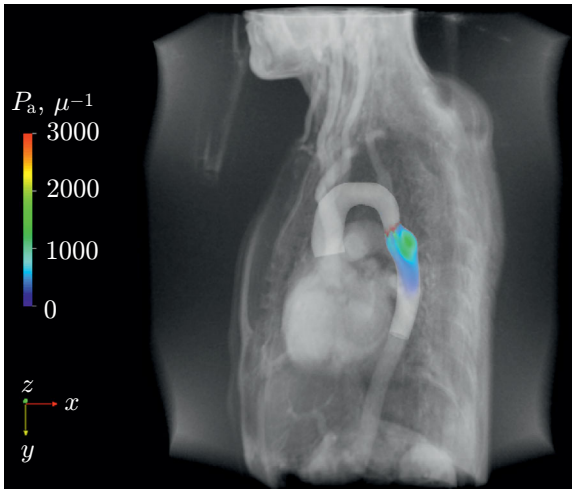

Fig. 2. The use of the developed facility for assessment of thrombus formation risks in the stenosed aorta. Imaging of the distribution of activated platelets in the stenosed aorta (volumetric blood flow $Q = 5.0$ l/min and $n = 80$) based on the volumetric rendering technology is presented. The red and blue colors correspond to the highest and the lowest concentrations of activated platelets in the considered area, respectively. The studies were performed according to the magnetic resonance angiography data, which are publicly available [82].

Figure 2 shows the calculated distribution of activated platelets in the aorta. It can be seen that platelets are activated in the vicinity of its lumen narrowing. The supercritical shear stresses that develop in the blood in this zone are the reason for this activation. Directly behind the stenosed area, there is a zone of recurrent flow, getting into which the activated platelets are able to provoke thrombus formation.

The given example of the calculation was performed for a particular degree of multimericity ($n = 80$). The distribution of VWF molecules is heterogeneous within the physiological norm, and the degree of multimericity usually does not exceed 80. The dependence of the platelet activation degree on the multimericity degree for physiological values of blood flow through the aorta was constructed to determine the contribution of multimers of different lengths to platelet activation.

The calculated dependences of the platelet activation degree on the number n of monomers in the VWF molecules for two values of the average volumetric blood flow are shown in Fig. 3. It is easy to see that the degree of platelet activation for large VWF molecules is considerably higher than for small ones, and the approximation lines *1* and *2* corresponding to two values of the average volumetric blood flow have a different slope.

The calculation results presented in Fig. 3 show that for any given level of blood flow through the descending aorta, VWF molecules with a multimericity below a certain level do not contribute to platelet activation at all (for high and low values of the flow Q, the contribution is not made by molecules smaller than 38 and 50 monomers, respectively). The degree of platelet activation by VWF multimers of supercritical size increases linearly with increasing multimericity.

In real systems, the degree of multimericity can be regulated by ADAMTS-13 metalloproteinase, which splits VWF molecules into smaller fragments. In the light of the obtained results, this means that the platelet activation level should decrease as a result of the ADAMTS-13 action, and in deep proteolysis, when the fragments of VWF molecules are less than the critical size in their multimericity, platelet activation should not occur under their influence at all.

4.2. Assessment of shear-induced platelet activation risks in mechanical circulatory assist devices

Activation of thrombus formation in intense shear flows is a serious problem not only in large arteries with pathologies, but also in blood-contacting devices used in transplantology (in particular, in mechanical circulatory assist devices) [83–85]. These include, in particular, cardiopulmonary bypass devices developed for the first time by C. C. Bryukhonenko [86], as well as mechanical circulatory assist devices (MCAD) used to compensate partially for violations of the heart pumping function [87, 88]. The use of the MCAD provided a breakthrough in the treatment of patients with chronic cardiac failure [89–91].

Unfortunately, the positive effect of using MCAD is largely offset by the high frequency of thromboembolic complications, primarily strokes. Clinical studies show that 45% of the patients had a stroke within two years [92, 93]. It is assumed that the supercritical shear stresses developing in the MCAD ($\tau > 1000\,\mathrm{dyn/cm^2}$) cause intense platelet activation, leading to the further formation of micro clots [94, 95].

Progress in the development of mathematical models aimed at assessing platelet shear activation risks has become especially notable in recent years [96–99]. From an applied point of view, the most interesting models are those that have been validated in a certain way [100] (i. e., for which their practical applicability has convincingly been demonstrated).

The issue of validation of mathematical models has recently attracted enhanced attention of both the scientific community (physicians, biomechanics, etc.) and regulators who control the quality of medical devices [101, 102]. The collaborative work of the American Society of Mechanical Engineers and the U.S. Food and Drug Administration (FDA) resulted in the development of a standard [103] describing common requirements for mathematical models that claim to be practical. In addition to the standard, the FDA also provided access to geometric parameters of two reference devices (see Fig. 4) [104]. Their use in the modeling of shear-induced platelet activation processes should ensure comparability of the results obtained by different research teams.

The developed facility for thrombus formation risk assessment was used to estimate the potential thrombogenicity of the reference models presented by the FDA.

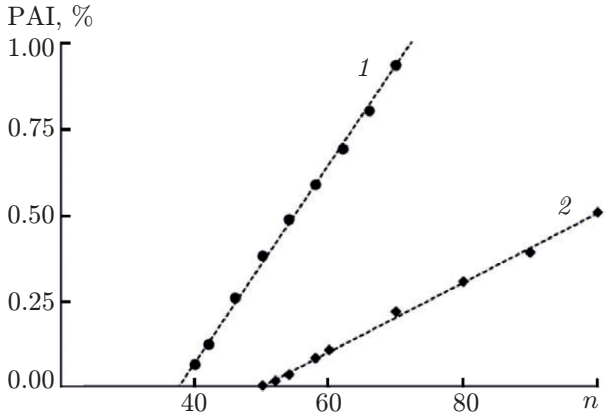

Fig. 3. The dependence of the platelet activation degree on the number n of monomers in the VWF molecules in the stenosed aorta for two values of the average volume flow, namely, $Q = 5.0$ l/min (*1*) and $Q = 3.7$ l/min (*2*). The degree of activation was defined as the cardiac-cycle averaged fraction of activated platelets at the exit from the aorta. The maximum degree of the luminal narrowing, calculated according to the diameter d of the descending aorta ($d = 2.5$ cm), was approximately 30%.

4.2.1. Assessment of platelet activation in the FDA Nozzle Benchmark Model test devices

The first reference model, the FDA Nozzle Benchmark Model, has geometry features typical of blood-contacting devices such as catheters, cannulas, and syringes. The model includes a converging section that turns into a uniform cross section and abrupt extension (see Fig. 4*a*). Such a structure contains zones of low and high shear stresses and zones of a positive pressure gradient that can destabilize the flow and form recirculation zones. These flow features are typical of the flow in blood-contacting devices and are characterized by increased thrombogenicity.

As a result of using the thrombus formation risk assessment facility, it was found out that the platelet activation zones in this model concentrate along the walls of the converging section and uniform cross section (see Fig. 5*b*). Increased shear-stress values in this zone develop due to the fluid acceleration in accordance with the incompressibility condition. In the zone of abrupt extension, a toroidal region of high stresses is formed, the amplitude of which exceeds the value required for activation (Fig. 5*a*). However, our calculations showed that these zones make an insignificant contribution to platelet activation. The main contribution comes from shear stresses occurring in the zones of the converging section and uniform cross section. Platelets moving along the device under study first pass through the narrowing region and the region of the smallest cross section, where they have time to pass to the primed for activation state. Based on the obtained results, it can be concluded that when Nozzle-type devices are designed, the geometry of these two regions should be adjusted in order to reduce the platelet activation level.

The dependence of the platelet activation degree on the Reynolds number in the place of the greatest narrowing of the vessel, obtained as a result of calculations, is shown in Fig. 6. The data presented in it show that the platelet activation degree in the range (to which the developers pay much attention) of the Reynolds number values increases from 12% to 14%. The obtained result indicates that a decrease in the blood flow intensity within the operating range will reduce only slightly the thrombogenicity of the devices of the considered type.

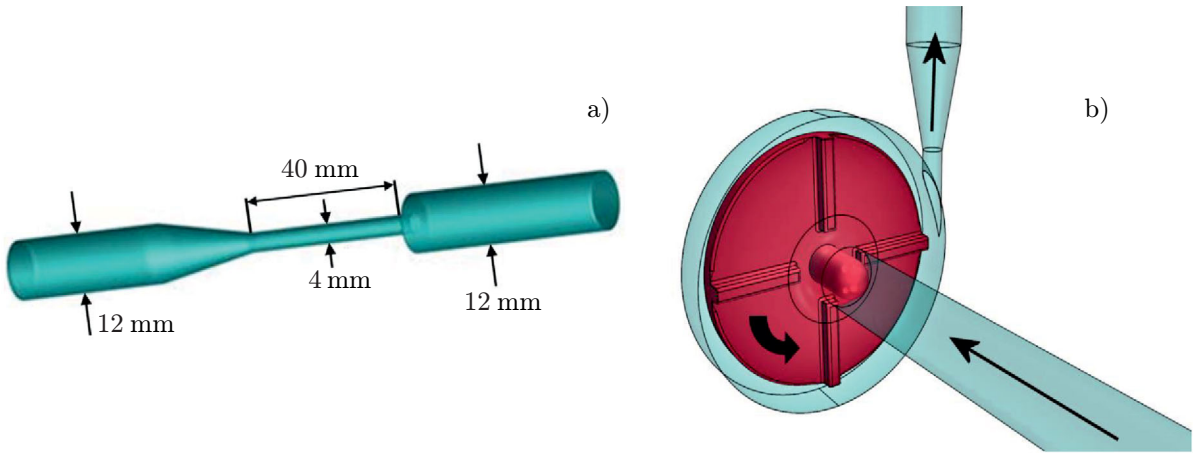

Fig. 4. Reference models developed by the FDA commission. (*a*) FDA Nozzle Benchmark Model is a prototype blood-contact device that repeats key features of the geometries of catheters, cannulas, and syringes. (*b*) FDA Blood Pump Benchmark Model is a prototype device that is a model of a mechanical circulatory assist device. Adapted from [104].

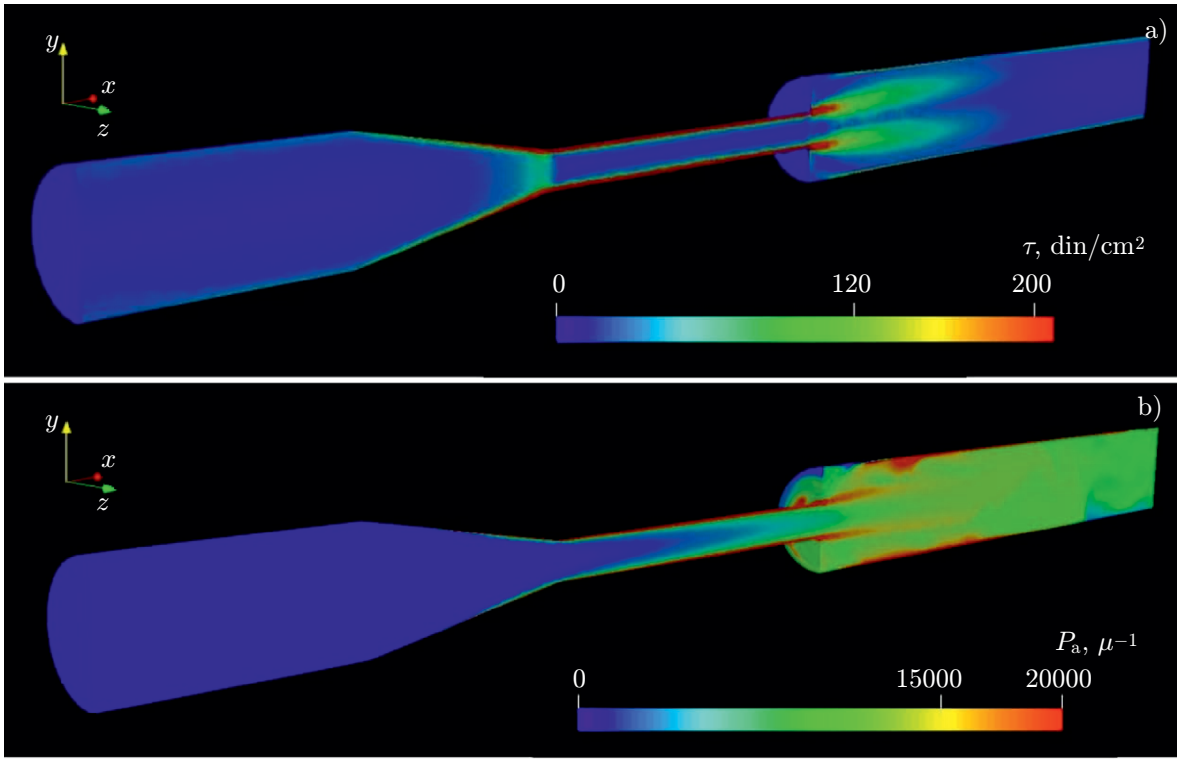

Fig. 5. Calculated shear stress distributions (*a*) and activated platelet concentrations (*b*) in the FDA Nozzle Benchmark Model. The red and blue colors correspond to the highest and the lowest concentrations of activated platelets in the considered area, respectively.

4.2.2. Assessment of platelet activation in FDA Blood Pump Benchmark Model test devices

The FDA Blood Pump Benchmark Model is an MCAD model (see Fig. 4*b*). The use of the thrombus formation risk assessment facility showed that increased shear stresses occur near the blades that set the blood in motion, as well as at the exit from the device body (see Fig. 7*a*). According to our calculations, there should be a volume activation of platelets in these zones. The final level of platelet activation in

this pump, unlike the FDA Nozzle Benchmark Model, is determined primarily by the size of the volume activation zones.

There is some experimental evidence that the proteolysis of VWF molecules by the ADAMTS-13 enzyme is accelerated in a turbulent flow [105, 106]. However, the platelet activation level in the MCAD varies only slightly [107]. This indicates that platelet activation mechanisms that are not related to VWF molecules can probably occur in turbulent flows. This range of issues requires further study.

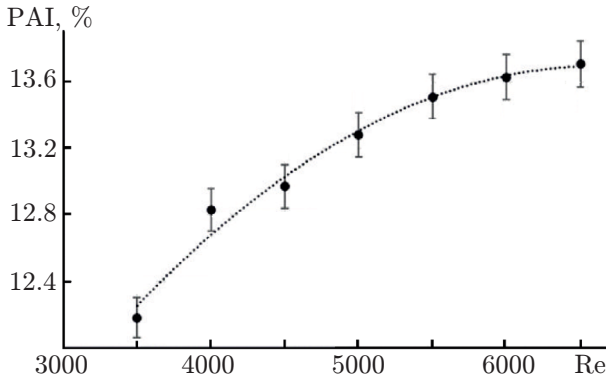

Fig. 6. The dependence of the platelet activation degree on the Reynolds number in the region of the maximum luminal narrowing in the protorype FDA Nozzle Benchmark Model ($n = 30$). The dotted line corresponds to the approximating curve.

The calculations showed that in the considered FDA Blood Pump Benchmark Model, a significant activation of platelets can indeed take place in a wide range of operating parameters. This conclusion qualitatively correlates with the well-known clinical observation on the unsafe use of this type of construction in practice [93]. Seeking more advanced structures is currently the subject of research of specialists in the field of biomedicine around the world [108, 109].

5. PROMISING APPLIED FIELDS

5.1. Assessment of individual risks of thrombus formation activation in clinical settings

Modern CFD methods in combination with medical information imaging techniques are used to develop software and hardware systems for both diagnostic and prognostic goals in cardiology and cardiovascular surgery [110, 111]. To date, the FDA has approved a number of software products and devices for clinical use in the diagnosis of cardiovascular pathologies (Software as Medical Device) [111]. One of these software products is HeartFlow for assessment of the fractional flow reserve (FFR) in the coronary arteries [112]. The value of the fractional reserve reflects the degree of supply of the myocardium with blood in heart diseases. The FDA-approved HeartFlow software product helps the physicians estimate the FFR value, and also predict its change after reconstructive treatment.

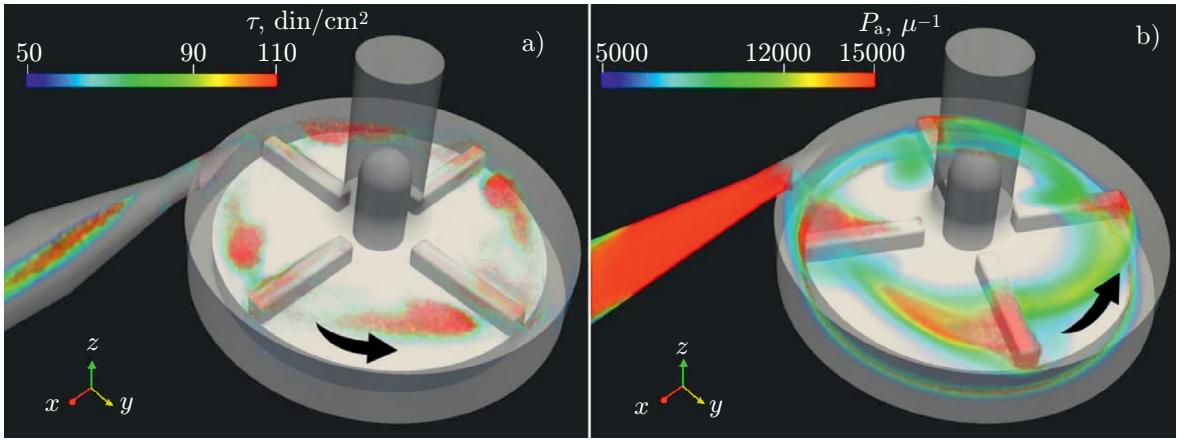

Fig. 7. Calculated shear stress distributions (*a*) and activated platelet concentrations (*b*) in the FDA Blood Pump Benchmark Model (rotation speed 1000 r/s, $Q = 0.5$ l/min, and $n = 30$). The black arrows indicate the rotor spin direction of the prototype mechanical circulatory assist device. The red and blue colors correspond to the highest (platelet activation 15%) and the 5% concentration of activated platelets, respectively.

However, despite the progress in the field of hemodynamic modeling, the existing software products preclude the assessment of intravascular thrombus formation risks. To estimate the thrombogenicity of large vessels, it was necessary to allow for the contribution of the hydrodynamic effects to the platelet volume activation. The developed approach is already able to assess these risks for a particular patient in a few days. In this case, the speed of obtaining estimates is determined mainly by the calculating capacity of the computers currently used. The pace of development of computer technologies and CFD methods assures that intravascular thrombus formation risks can be assessed in no more than a few hours in the near future [113]. In prospect, this will give physicians an opportunity to use a method based on the developed approach to assess the thrombogenicity risks due to platelet activation in operational decision-making in clinical situations.

It is worth noting that, in addition to the mechanisms of thrombus formation due to the volumetric shear-induced platelet activation (platelet link of hemostasis), violations of the integrity of the vascular walls (vascular link of hemostasis) can play a significant role in the change of the blood aggregate state. Within the physiological norm, the endothelial cells lining the vessels from the inside maintain the blood in a liquid state due to the secretion of plasma and platelet inhibitors of hemostasis into the blood flow [29, 114, 115].

The permeability of the endothelium to procoagulants varies significantly in a number of clinical situations [116–118]. In particular, such variations can be provoked by an increase in tangential shear stresses acting on endothelial cells. At the same time, an increase in the supply of procoagulants to the parietal layers of the blood flow causes further blood coagulation activation [4]. These parietal mechanisms are implemented at moderate shear rates, up to $10^3\,\mathrm{s}^{-1}$, as a result of which the formation of blood clots is mainly determined by the vascular and plasma components of hemostasis [119].

In this paper, we have limited ourselves to considering the mechanisms of blood clot formation caused by disorders of the platelet hemostasis under the influence of shear stresses. Indeed, the volume activation of platelets can take place in large arteries [5, 120, 121]. It seems to us that the contribution of volume effects to the overall activation level should dominate over the surface (wall) effects. This hypothesis requires further analysis, including proof-of-concept experiments (see, i. e., [6, 122]).

Taking the volumetric platelet activation effects into account is of interest in cases where there is a significant increase in systolic blood pressure. The fact is that due to an increase in systolic pressure, the shear stresses in the blood flow can increase above the critical level, which, in turn, will be accompanied by platelet activation.

The degree of platelet activation of a particular person depends on the state of the cardiovascular system (the diameter of the vessels, the size of the cardiac output, and the presence of stenotic areas). In this case, the maximum value of shear stresses that are dangerous from the point of view of shear-induced platelet activation of a particular person depends on the features of systemic hemodynamics, including the value of systolic blood pressure. The developed approach enables one to estimate the maximum allowed value of systolic blood pressure in a personalized way. In cases where the systolic pressure exceeds this limit value, platelet activation should take place. The software and hardware system makes it possible to estimate the platelet activation intensity for a supercritical systolic pressure and thus to judge the thrombogenicity trends.

5.2. Ways to reduce the thrombogenicity of mechanical circulatory assist devices

The developed approach can also be used to assess thrombogenicity in vascular systems containing artificial elements, such as vascular implants (stents) and MCAD. The latter are widely used in medicine, but their application is related to a significant increase in the thrombus formation risk. Thrombus formation activation due to the use of MCAD can lead both to the failure of the devices themselves, and to the development of life-threatening pathological conditions, strokes in particular [95, 107, 123]. Several computational methods for assessing the MCAD thrombogenicity level are discussed in [96–99, 124]. However, none of them has yet been employed for the development and testing of new devices [125, 126]. Questions about the limits to which one can rely on mathematical models and their computer implementations are discussed in

professional circles, and the concept of model credibility risk has appeared [127].

It seems that today the issues of the applicability limits of models in describing the blood dynamics have most thoroughly been considered in a series of papers [102, 128], which study the effect of shear stresses on the hemolysis of erythrocytes in the MCAD. The developed models are based on the concepts of a mechanical tear of erythrocytes. They are constructed [128] using the V&V 40 standard [103]. Their authors assume that hemolysis is initiated in a threshold manner [129, 130]. As a result, the developed approach is of interest from a methodological point of view.

Since platelet activation also belongs to the class of threshold phenomena [131, 132], it stands to reason to allow for the requirements of the V&V 40 standard [103] in the development of the existing models in the future. Application of this standard will open up the possibility of selecting platelet activation models that best meet the FDA requirements. The improvement of the currently used approaches to assessing the thrombus formation activation in accordance with the FDA requirements will be able to move from testing individual mock-up samples to adjusting the industrial programs for the development and design of advanced MCADs. The result of this is expected to be a reduction in the number of thrombotic complications caused by the use of MCAD.

5.3. Development of wearable hemostasis correction devices

The use of mathematical models that have passed the validation procedure will make it possible to calculate estimates of the thrombus formation risks under conditions of a high blood flow. The availability of such estimates will give physicians the opportunity to reduce uncertainty when making decisions on the choice of dosages of antithrombotic drugs for particular patients [133].

The developed mathematical approaches permit one to compare the thrombus formation risks not only with the variation of dosages, but also with changes in the drug administration protocols [5, 134]. In cases where drugs are administered gradually (as in the case of heparin administration), such effects can be taken into account as parametric in the model. However, in addition to the provision of directed parametric effects, questions about the provision of operational (dynamic) effects on the hemostatic system deserve attention. The goal of such an impact is to abruptly stop the transient processes of thrombus formation/thrombolysis in vital organs.

It is known that the effectiveness of drugs that dissolve fibrin clots (fibrinolytics) depends significantly on the phase of coagulation development at the time of their administration and dose [135, 136]. In this regard, it is necessary to develop devices for continuous monitoring of the hemostatic system state to stop thrombus formation in time. In [14, 137–139], the authors showed that the principle of operation of such devices for the correction of hemostasis can be based on the acoustic detection of micro clots. The advent of inexpensive micrometer-sized ultrasonic transmitters [140] has opened the way for using such devices in medical practice [141, 142]. Compact wearable or implantable devices capable of detecting micro clots at the early stages of thrombus formation will be able to calculate quickly (in real time) the dosages and instants of administration of fibrinolytics, as well as provide management of their timely injection to particular patients in the future [14].

It should be noted that to date, the FDA commission has approved both wearable and implantable devices for monitoring and correcting glucose levels in a human body [143, 144]. Such breakthroughs in the field of biomedical engineering give good reason to believe that the creation of compact wearable devices for the correction of hemostasis is a matter of the near future. Their use should reduce the level of mortality and disability that occur due to the rapid development of thrombus formation in large arteries.

Thus, modern methods of medical diagnostics (ultrasound, magnetic resonance imaging and computed tomography), combined with the achievements of computational fluid dynamics, open up wide opportunities for the development of a new generation of medical devices and software and hardware systems that are able not only to obtain information about the structure and current functional state of the organs and tissues under study, but also to predict the consequences of surgical and pharmacological treatments.

6. CONCLUSIONS

The analysis shows that as a result of the influence of shear stresses on the conformational dynamics of VWF macromolecules, significant activation of platelets can occur not only in *in vitro* systems and in mechanical circulatory assist devices (*ex vivo*), but also in large stenosed vessels (*in vivo*). The developed approach and the software and hardware system created on its basis are used to find the probability of volumetric shear-induced platelet activation in vessels that are isomorphic in their geometry to those present in a human body. The application of this approach makes it possible in principle to analyze the effect of both static [5] and dynamic (time-varying) shear stresses [76] on platelet activation.

It seems that the obtained results will give physicians the opportunity to plan an antithrombotic therapy strategy in the future, taking the individual risks of shear-induced platelet activation into account.

The paper was supported by the Russian Science Foundation (project No. 19-11-00260) and performed using the equipment of the collective-use center "System for modeling and data processing of mega-class research facilities" of the Kurchatov Institute (the Ministry of Science and Higher Education grant with identifier RFMEFI62117X0016; http://ckp.nrcki.ru/).

We express our gratitude to G. A. Yatsyk, the head of the Department of Magnetic Resonance Imaging and Ultrasound Diagnostics of the National Medical Research Center for Hematology, for providing the magnetic resonance angiography data used in this paper.

We express our gratitude to E. V. Gorina and S. N. Garichev, the Moscow Institute of Physics and Technology, for their assistance in organizing computational procedures.

APPENDIX 1

Programs, numerical methods, and parameter values

The aortic geometry was recovered on the basis of open-access magnetic resonance angiography data [82]. Image segmentation was performed at the first stage of the recovery to highlight the boundaries of the vascular lumen [145]. A polygonal surface approximating the geometry of the vessels was constructed at the second stage using the method of marching cubes [146]. To improve the convergence of the calculations, following [147], a cylindrical segment was added to the output section of the aorta. The length of the cylindrical segment was two times greater than the diameter of the output section. The recovery and processing of polygonal surfaces were performed using the open software product VMTK [148].

The internal volume of polygonal surfaces allowing for the personalized features of the vessel structure was filled with hexahedral elements. In the vicinity of the vessel walls, the cells were further reduced in order to resolve the boundary layer [149]. The calculated grids contained about 200000 elements and were constructed in the CF-MESH+ software product [150].

The dependence of the average blood flow rate at the entrance to the aorta on the time of the cardiac cycle (base profile) was adapted from [151]. To obtain the desired value of the average volumetric blood flow through the aorta, the base profile was adjusted with multiplying by the scaling factor r: $r = Q/Q_0$, where Q is the required average volumetric blood flow per cardiac cycle and Q_0 is the average volumetric blood flow per cardiac cycle for the base profile.

The geometry of the reference FDA models was constructed on the basis of the dimensions indicated in [128, 152]. Further, discretization of the internal volumes of the models was performed using tetrahedral elements with their local reduction in size near the walls. These procedures were conducted using the open source software Salome package [153].

Equations (3), (4), (7), (8), (12), and (15) were numerically solved by the finite volume method [80]. Approximation of the convective term in Eqs. (3), (7), (8), (12), (14), and (15) was performed by the counterflow difference method [154]. The time derivative in these equations was approximated using the implicit Euler method [80]. The velocity and pressure fields were found by solving Eqs. (3) and (4) (or Eq. (12) and (13)) using the PISO algorithm [155]. An adaptive time pitch, the size of which was calculated

TABLE A1.1. Values of the model parameters used to analyze the platelet activation risk.

Parameter	Physiological range	Reference	Used value
η, cP	3–4	[23]	4
ρ, g/cm^3	1.040–1.060	[161]	1.056
$\dot{\gamma}_c = \tau_c/\eta$, s^{-1}	1000–10000	[5]	10000
n_a	> 20	[73]	22
k, s^{-1}	no data	–	10000
Sc	no data	–	0.9

from the condition CFL< 1, where CFL is the Courant number [156], was employed.

When modeling turbulent flows, the level of turbulence at the entrance to the considered FDA reference models, following [128], was assumed to be equal to 1%. The $k-\omega-$SST model was used to find the turbulent kinematic viscosity field. When solving the equations of this model, the following boundary conditions were used on the walls of the calculated regions. The turbulent kinetic energy was assumed to be zero. The frequency of turbulent fluctuations was calculated using the automatic wall function method described in [157].

The sliding grid approach was used to calculate shear-induced activation in the FDA Blood Pump Benchmark Model [158]. In this approach, the rotating rotor and the stationary stator were separated by a double-sided interface. The equality of values for each calculated variable on the sides of the interface was the boundary condition.

The program code for solving the equations was written in the open environment OpenFOAM [159]. Visualization of the calculation results was performed in the ParaView environment [160]. The images were made in the Excel software product.

The values of the parameters used to analyze the platelet activation risk are presented in Table A1.1. When calculating the turbulent flows, the values of the parameters of the $k-\omega-$SST model were taken from [157].

The concentration of inactivated platelets at the entrance to the calculated areas was assumed to be equal to 200000 pcs/μ^{-1} in all calculations. The initial concentration of inactivated platelets in the calculated areas was assumed to be equal to the concentration at the entrance to the vessel. The initial concentration of activated platelets in the calculated areas was considered to be zero.

APPENDIX 2

Key stages of personalized research using CFD models

A personalized study in the field of cardiovascular modeling consists of several sequential steps (see Fig. A2.1).

At the first step (see Fig. A2.1*a*), the patient undergoes a radiological examination, e. g., computed tomography or magnetic resonance imaging of blood vessels [162]. The immediate result of tomography is a series of images containing information about the anatomical structure of blood vessels at different depths (a set of sections). It should be noted that both specific vessels (e. g., coronary arteries) and extensive vascular networks (e. g., Willis' circle arteries) can be examined.

At the next step (see Fig. A2.1*b*), the geometry of the vessels is recovered by marking out the vessel lumen (segmentation) on each section and then triangulating their internal surface [163–165]. To date, a number of software products for computed tomography and magnetic resonance angiography data processing is publicly available [148, 166]. Their use makes it possible to triangulate the inner surface of the vascular

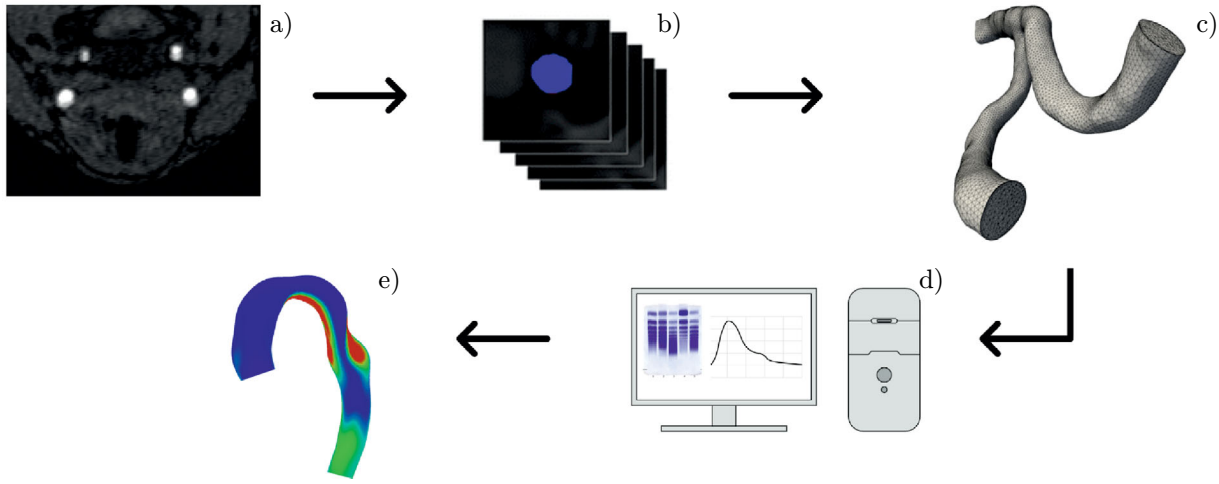

Fig. A2.1. The main stages of personalized research using CFD models. (*a*) Magnetic resonance angiography data without contrast enhancement (axial section). (*b*) Two-dimensional cross-sectional segmentation of the vascular lumen in the axial direction. (*c*) An example of the computational grid. (*d*) Calculations with allowance for additional information about the cardiovascular system state (e. g., the analysis of the multimericity of VWF molecules, the dependence of the volumetric blood flow on time, etc). (*e*) Visualization of the calculation results in the form of a video clip.

blood flow (see Appendix 1). The resulting surface grid reproduces the anatomical features of the vessels of interest.

At the third stage, a computational grid is created in the inner region of the assumed blood flow in the vessel (see Fig. A2.1*c*) [149]. Unstructured hybrid grids are used (see Appendix 1).

Computational grids are then used in computer experiments (see Fig. A2.1*d*). At the same time, mathematical simulation also allows for the data obtained in the laboratory and clinical studies (blood viscosity and volume flow rate within the cardiac cycle). All of this permits one to calculate the state of hemodynamics with allowance for personal data using the well-known CFD methods [110, 162] (see Appendix 1). In the course of procedures aimed at assessing the shear-induced thrombus formation risks, it is necessary to consider both the features of blood hemodynamics and the state of the hemostatic system as a whole, including data on the multimericity of VWF molecules [167].

The last stage of work is the preparation of calculation results in the form of presentation videos (see Fig. A2.1*e*). This is done by using 3D imaging methods which clearly demonstrate the dynamics of the studied processes [160] (see Appendix 1).

REFERENCES

1. M. T. Grekhova, ed.,*Autowave Processes in Systems with Diffusion* [in Russian], Inst. Appl. Phys. Gorky (1981).
2. A. V. Panfilov, H. Dierckx, and V. Volpert, *Physica D*, **399**, 1–34 (2019). https://doi.org/10.1016/j.physd.2019.04.001
3. K. G. Guria and G. Th. Guria, *Thromb. Res.*, **135**, No. 3, 423–433 (2015). https://doi.org/10.1016/j.thromres.2014.12.014
4. O. S. Rukhlenko, O. A. Dudchenko, K. E. Zlobina, and G. T. Guria, *PLOS ONE*, **10**, No. 7, e0134028 (2015). https://doi.org/10.1371/journal.pone.0134028
5. K. E. Zlobina and G. T. Guria, *Sci. Rep.*, **6**, 30508 (2016). https://doi.org/10.1038/srep30508
6. S. Rahman, A. Fogelson, and V. Hlady, *Colloids Surf. B. Biointerfaces*, **193**, 111118 (2020). https://doi.org/10.1016/j.colsurfb.2020.111118

7. V. T. Turitto and C. L. Hall, *Thromb. Res.*, **92**, No. 6, S25–S31 (1998). https://doi.org/10.1016/s0049-3848(98)00157-1

8. D. M. Wootton and D. N. Ku, *Annu. Rev. Biomed. Eng.*, **1**, 299–329 (1999). https://doi.org/10.1146/annurev.bioeng.1.1.299

9. O. V. Rudenko, *Phys. Usp.*, **50**, No. 4, 359–367 (2007). https://doi.org/10.1070/PU2007v050n04ABEH006236

10. W. Drexler and J. G. Fujimoto, eds., *Optical Coherence Tomography: Technology and Applications. 2nd ed.*, Springer, Cham (2015).

11. E. A. Shirshin, Y. I. Gurfinkel, A. V. Priezzhev, et al., *Sci. Rep.*, **7**., 1171, 1–10 (2017). https://doi.org/10.1038/s41598-017-01238-w

12. G.-H. Jahng, K.-L. Li, L. Ostergaard, et al., *Korean J. Radiol.*, **15**, No. 5, 554–577 (2014). https://doi.org/10.3348/kjr.2014.15.5.554

13. S. Zhang, A. A. Joseph, D. Voit, et al., *Quant. Imaging Med. Surg.*, **4**, No. 5, 313–329 (2014). https://doi.org/10.3978/j.issn.2223-4292.2014.06.03

14. D. A. Ivlev, S. N. Shirinli, K. G. Guria, et al., *PLOS ONE*, **14**, No. 2, e0211646 (2019). https://doi.org/10.1371/journal.pone.0211646

15. L. Formaggia, A. Quarteroni, and A. Veneziani, eds., *Cardiovascular Mathematics: Modeling and Simulation of the Circulatory System, Vol. 1*, Springer, Berlin (2009).

16. V. B. Koshelev, S. I. Mukhin, N. V. Sosnin, and A. P. Favorsky, *Mathematical Models of Quasi-One-Dimensional Hemodynamics* [in Russian], MAKS Press, Moscow (2010).

17. N. Bessonov, A. Sequeira, S. Simakov, et al., *Math. Model. Nat. Phenom.*, **11**, No. 1, 1–25 (2016). https://doi.org/10.1051/mmnp/201611101

18. D. A. Steinman and C. A. Taylor, *Ann. Biomed. Eng.*, **33**, No. 12, 1704–1709 (2005). https://doi.org/10.1007/s10439-005-8772-2

19. D. V. Parshin, Y. O. Kuyanova, D. S. Kislitsin, et al., *J. Appl. Mech. Tech. Phys.*, **59**, No. 6, 963–970 (2018). https://doi.org/10.1134/S0021894418060019

20. C. G. Caro, T. J. Pedley, R. C. Schroter, and W. A. Seed, *The Mechanics of the Circulation*, Cambridge Univ. Press, Cambridge (2012).

21. J. Tu, K. Inthavong, and K. K. L. Wong, *Computational Hemodynamics: Theory, Modeling and Applications*, Springer, Dordrecht (2015).

22. A. Fasano and A. Sequeira, *Hemomath: The Mathematics of Blood*, Springer, Cham (2017).

23. R. F. Schmidt and G. Thews, ed., *Human Physiology*, Springer–Verlag, Berlin–Heidelberg (1989). https://doi.org/10.1007/978-3-642-73831-9

24. H. L. Goldsmith and V. T. Turitto, *J. Thromb. Haemost.*, **56**, No. 3, 415–435 (1986).

25. T. G. Papaioannou and C. Stefanadis, *Hellenic J. Cardiol.*, **46**, No. 1, 9–15 (2005).

26. L. F. Brass and S. L. Diamond, *J. Thromb. Haemost.*, **14**, No. 5, 906–1117 (2016). https://doi.org/10.1111/jth.13280

27. A. M. Mel'kumyants and S. A. Balashov, *Arterial Endothelium Mechanosensitivity* [in Russian], Triada, Moscow (2005).

28. M. H. Kroll, J. D. Hellums, L. V. McIntire, et al., *Blood*, **88**, No. 5, 1525–1541 (1996).

29. A. V. Mazurov, *Platelet Physiology and Pathology* [in Russian], Literra, Moscow (2011).

30. L. J. Wurzinger, R. Opitz, P. Blasberg, and H. Schmid-Schänbein, *J. Thromb. Haemost.*, **53**, No. 2, 381–386 (1985). https://doi.org/10.1055/s-0038-1657744

31. C. Zhang, A. Kelkar, and S. Neelamegham, *Blood Adv.*, **3**, No. 7, 957–968 (2019). https://doi.org/10.1182/bloodadvances.2018030122

32. D. Katritsis, L. Kaiktsis, A. Chaniotis, et al., *Prog. Cardiovasc. Dis.*, **49**, No. 5, 307–329 (2007). https://doi.org/10.1016/j.pcad.2006.11.001

33. P. Dyverfeldt, M. Bissell, A. J. Barker, et al., *J. Cardiovasc. Magn. Reson.*, **17**, No. 1, 72 (2015). https://doi.org/10.1186/s12968-015-0174-5

34. E. Heiberg, J. Sjögren, M. Ugander, et al., *BMC Med. Imaging*, **10**, No. 1, 1 (2010). https://doi.org/10.1186/1471-2342-10-1

35. M. Markl, A. Frydrychowicz, S. Kozerke, et al., *J. Magn. Reson. Imaging*, **36**, No. 5, 1015–1036 (2012). https://doi.org/10.1002/jmri.23632

36. L. Boussel, V. Rayz, A. Martin, et al., *Magn. Reason. Med.*, **61**, No. 2, 409–417 (2009). https://doi.org/10.1002/mrm.21861

37. J. Szajer and K. Ho-Shon, *J. Magn. Reson. Imaging*, **48**, 62–69 (2018). https://doi.org/10.1016/j.mri.2017.12.005

38. G. T. Guria, *Kommers. Nauka*, **9**, No. 9, 50–57 (2011).

39. A. L. Chulichkov, A. V. Nikolayev, A. I. Lobanov, and G. T. Guria, *Mat. Model.*, **12**, No. 3, 75–96 (2000).

40. A. P. Guzevatykh, A. I. Lobanov, and G. T. Guria, *Mat. Model.*, **12**, No. 4, 39–60 (2000).

41. A. Lobanov and T. Starozhilova, *Pathophysiol. Haemost. Thromb.*, **34**, Nos. 2–3, 121–134 (2005). https://doi.org/10.1159/000089932

42. D. Basmadjian, M. Sefton, and S. Baldwin, *Biomaterials*, **18**, No. 23, 1511–1522 (1997). https://doi.org/10.1016/S0142-9612(97)80002-6

43. A. L. Fogelson and R. D. Guy, *Math. Med. Biol.*, **21**, No. 4, 293–334 (2004). https://doi.org/10.1093/imammb/21.4.293

44. S. Cito, M. D. Mazzeo, and L. Badimon, *Thromb. Res.*, **131**, No. 2, 116–124 (2013). https://doi.org/10.1016/j.thromres.2012.11.020

45. M. Anand and K. R. Rajagopal, *Fluids*, **2**, No. 3, 35 (2017). https://doi.org/10.3390/fluids2030035

46. S. Yesudasan and R. D. Averett, *Comput. Biol. Chem.*, **83**, 107148 (2019). https://doi.org/10.1016/j.compbiolchem.2019.107148

47. F. Shen, C. J. Kastrup, Y. Liu, and R. F. Ismagilov, *Arterioscler. Thromb. Vasc. Biol.*, **28**, No. 11, 2035–2041 (2008). https://doi.org/10.1161/ATVBAHA.108.173930

48. A. I. Vorob'ev, V. M. Gorodetsky, E. M. Shuludko, and S. A. Vasyl'ev, *Sharp Massive Blood Loss* [in Russian], GEOTAR-MED, Moscow (2001).

49. D. Zipes, P. Libby, R. Bonow, et al., eds., *Braunwald's Heart Disease: A Textbook of Cardiovascular Medicine. 11th ed.*, WB Saunders Company, Philadelphia (2018).

50. Z. M. Ruggeri, *Thromb. Haemost.*, **70**, No. 1, 119–123 (1993).

51. A. Michelson, ed., *Platelets. 3rd ed.*, Academic Press, Amsterdam (2013).

52. S. Goto, Y. Ikeda, E. Saldívar, and Z. M. Ruggeri, *J. Clin. Invest.*, **101**, No. 2, 479–486 (1998). https://doi.org/10.1172/JCI973

53. H. Shankaran, P. Alexandridis, and S. Neelamegham, *Blood*, **101**, No. 7, 2637–2645 (2003). https://doi.org/10.1182/blood-2002-05-1550

54. I. Singh, E. Themistou, L. Porcar, and S. Neelamegham, *Biophys. J.*, **96**, No. 6, 2313–2320 (2009). https://doi.org/10.1016/j.bpj.2008.12.3900

55. L. D. C. Casa, D. H. Deaton, and D. N. Ku, *J. Vasc. Surg.*, **61**, No. 4, 1068–1080 (2015). https://doi.org/10.1016/j.jvs.2014.12.050

56. D. Kim, C. Bresette, Z. Liu, and D. N. Ku, *APL Bioeng.*, **3**, No. 4, 041502 (2019). https://doi.org/10.1063/1.5115554

57. V. Huck, M. F. Schneider, C. Gorzelanny, and S. W. Schneider, *J. Thromb. Haemost.*, **111**, No. 4, 598–609 (2014). https://doi.org/10.1160/TH13-09-0800

58. Y. Jiang, H. Fu, T. A. Springer, and W. P. Wong, *J. Mol. Biol.*, **431**, No. 7, 1380–1396 (2019). https://doi.org/10.1016/j.jmb.2019.02.014

59. A. Rana, E. Westein, B. E. Niego, and C. E. Hagemeyer, *Front. Cardiovasc. Med.*, **6**, 141 (2019). https://doi.org/10.3389/fcvm.2019.00141

60. Y. Qiu, J. Ciciliano, D. R. Myers, et al., *Blood Rev.*, **29**, No. 6, 377–386 (2015). https://doi.org/10.1016/j.blre.2015.05.002

61. E. Di Stasio and R. De Cristofaro, *Biophys. Chem.*, **153**, No. 1, 1–8 (2010). https://doi.org/10.1016/j.bpc.2010.07.002

62. H. Horiuchi, T. Doman, K. Kokame, et al., *J. Atheroscler. Thromb.*, **26**, No. 4, 303–314 (2019). https://doi.org/10.5551/jat.RV17031

63. R. K. Andrews, J. López, and M. C. Berndt, *Int. J. Biochem. Cell. Biol.*, **29**, No. 1, 91–105 (1997). https://doi.org/10.1016/S1357-2725(96)00122-7

64. N. A. Mody and M. R. King, *Biophys. J.*, **95**, No. 5, 2556–2574 (2008). https://doi.org/10.1529/biophysj.107.128520

65. T. A. Springer, *Blood*, **124**, No. 9, 1412–1425 (2014). https://doi.org/10.1182/blood-2014-05-378638

66. S. W. Schneider, S. Nuschele, A. Wixforthet, et al., *PNAS*, **104**, No. 19, 7899–7903 (2007). https://doi.org/10.1073/pnas.0608422104

67. S. Gogia and S. Neelamegham, *Biorheology*, **52**, Nos. 5–6, 319–335 (2015). https://doi.org/10.3233/BIR 15061

68. A. Löf, J. P. Müller, and M. A. Brehm, *J. Cell. Physiol.*, **233**, No. 2, 799–810 (2018). https://doi.org/10.1002/jcp.25887

69. R. M. Vergauwe, H. Uji-i, K. De Ceunynck, et al., *J. Phys. Chem. B.*, **118**, No. 21, 5660–5669 (2014). https://doi.org/10.1021/jp5022664

70. S. Lancellotti, M. Sacco, M. Basso, and R. De Cristofaro, *Biomol. Concepts*, **10**, No. 1, 194–208 (2019). https://doi.org/10.1515/bmc-2019-0022

71. S. Goto, D. R. Salomon, Y. Ikeda, and Z. M. Ruggeri, *J. Clin. Chem.*, **270**, 23352–23361 (1995). https://doi.org/10.1074/jbc.270.40.23352

72. J. L. Moake, N. A. Turner, N. A. Stathopoulos, et al., *J. Clin. Invest.*, **78**, No. 6, 1456–1461 (1986). https://doi.org/10.1172/JCI112736

73. M. Stockschlaeder, R. Schneppenheim, and U. Budde, *Blood Coagul. Fibrinolysis*, **25**, No. 3, 206–216 (2014). https://doi.org/10.1097/MBC.0000000000000065

74. A. J. Reininger, *Hämostaseologie*, **35**, No. 3, 225–233 (2015). https://doi.org/10.5482/HAMO-14-12-0077

75. A. Alexander-Katz and R. R. Netz, *Macromolecules*, **41**, No. 9, 3363–3374 (2008). https://doi.org/10.1021/ma702331d

76. D. M. Pushin, T. Y. Salikhova, K. E. Zlobina, and G. Th. Guria, *PLOS ONE*, **15**, No. 6, e0234501 (2020). https://doi.org/10.1371/journal.pone.0234501

77. G. K. Batchelor, *An Introduction to Fluid Dynamics*, Cambridge Univ. Press, Cambridge (2000).

78. K. Tesch, *Task Quarterly*, **17**, Nos. 3–4, 1000–1008 (2013).

79. D. C. Wilcox, *Turbulence Modeling for CFD*, DCW Industries, California (2006).

80. J. Ferziger, M. Perić, and R. Street, eds., *Computational Method for Fluid Dynamics. 4th ed.*, Springer, Cham (2020).

81. F. R. Menter, *AIAA J.*, **32**, No. 8, 1598–1605 (1994).

82. https://www.osirix-viewer.com/resources/dicom-image-library/

83. M. Q. Najib, R. K. Wong, C. N. Pierce, et al., *Eur. Heart J. Cardiovasc. Imaging.*, **13**, No. 6, 532 (2012). https://doi.org/10.1093/ehjci/jes011

84. M. Capoccia, C. T. Bowles, A. Sabashnikov, and A. Simon, *J. Investig. Med. High Impact Case Rep.*, **1**, No. 2, 2324709613490676 (2013). https://doi.org/10.1177/2324709613490676

85. J. K. Kirklin, D. C. Naftel, F. D. Pagani, et al., *J. Heart Lung Transpl.*, **34**, No. 12, 1515–1526 (2015). https://doi.org/10.1016/j.healun.2015.10.024

86. S. S. Brukhonenko, *Sbornik Tr. Inst. Éksp. Fiziol. Terapii*, No. 1, 32–34 (1937).

87. S. V. Gautier, G. P. Itkin, A. O. Shevchenko, et al., *Vestnik Transplant. Iskusstv. Org.*, **18**, No. 3, 128–136 (2016). https://doi.org/10.15825/1995-1191-2016-3-128-136

88. B. B. Chung, G. Sayer, and N. Uriel, *Expert Rev. Med. Dev.*, **14**, No. 5, 343–353 (2017). https://doi.org/10.1080/17434440.2017.1324292

89. J. N. Kirkpatrick, G. Wieselthaler, M. Strueber, et al., *Heart*, **101**, 1091–1096 (2015). https://doi.org/10.1136/heartjnl-2014-306789

90. G. P. Itkin, A. S. Buchnev, A. P. Kuleshov, and A. I. Syrbu, *Vestnik Transplant. Iskusstv. Org.*, **21**, No. 1, 71–76 (2019). https://doi.org/10.15825/1995-1191-2019-1-71-76

91. R. J. Miller, J. J. Teuteberg, and S. A. Hunt, *Annu. Rev. Med.*, **70**, 33–44 (2019). https://doi.org/10.1146/annurev-med-041217-011015

92. S. S. Najjar, M. S. Slaughter, F. D. Pagani, et al., *J. Heart Lung Transpl.*, **33**, No. 1, 23–34 (2014). https://doi.org/10.1016/j.healun.2013.12.001

93. W. K. Cornwell III, A. V. Ambardekar, T. Tran, et al., *Stroke*, **50**, No. 2, 542–548 (2019). https://doi.org/10.1161/STROKEAHA.118.022967

94. D. Bluestein, Y. M. Li, and I. B. Krukenkamp, *J. Biomech.*, **35**, No. 12, 1533–1540 (2002). https://doi.org/10.1016/S0021-9290(02)00093-3

95. M. J. Slepian, J. Sheriff, M. Hutchinson, et al., *J. Biomech.*, **50**, 20–25 (2017). https://doi.org/10.1016/j.jbiomech.2016.11.016

96. G. Girdhar, M. Xenos, Y. Alemu, et al., *PLOS ONE*, **7**, No. 3, e32463 (2012). https://doi.org/10.1371/journal.pone.0032463

97. W. T. Wu, F. Yang, J. Wu, et al., *Sci. Rep.*, **6**, 38025 (2016). https://doi.org/10.1038/srep38025

98. G. Fuchs, N. Berg, L. M. Broman, and L. P. Wittberg, *Sci. Rep.*, **9**, 8809 (2019). https://doi.org/10.1038/s41598-019-45121-2

99. W. C. Chiu, P. L. Tran, Z. Khalpey, et al., *Sci. Rep.*, **9**, 2946 (2019). https://doi.org/10.1038/s41598-019-39897-6

100. P. Pathmanathan, R. A. Gray, V. J. Romero, and T. M. Morrison, *J. Verif. Valid. Uncertain. Quantif.*, **2**, No. 2, 021005 (2017). https://doi.org/10.1115/1.4037671

101. A. Blitz, *Ann. Cardiothorac. Surg.*, **3**, No. 5, 450–471 (2014). https://doi.org/10.3978/j.issn.2225 319X.2014.09.10

102. T. M. Morrison, P. Hariharan, C. M. Funkhouser, et al., *ASAIO J.*, **65**, No. 4, 349–360 (2019). https://doi.org/10.1097/MAT.0000000000000996

103. https://cstools.asme.org/csconnect/CommitteePages.cfm?Committee=100108782

104. R. A. Malinauskas, P. Hariharan, S. W. Day, et al., *ASAIO J.*, **63**, No. 2, 150–160 (2017). https://doi.org/10.1097/MAT.0000000000000499

105. C. Jhun, C. Siedlecki, L. Xu, et al., *Artif. Organs*, **43**, No. 2, 199–206 (2018). https://doi.org/10.1111/aor.13323

106. M. Bortot, K. Ashworth, A. Sharifi, et al., *Arterioscler. Thromb. Vasc. Biol.*, **39**, No. 9, 1831–1842 (2019). https://doi.org/10.1161/ATVBAHA.119.312814

107. Z. Chen, A. Sun, and H. Wang, et al., *Medicine Novel Tech. Dev.*, **3**, 100024 (2019). https://doi.org/10.1016/j.medntd.2019.100024

108. A. L. Marsden, Y. Bazilevs, C. C. Long, et al., *Wiley Interdiscip. Rev. Syst. Biol. Med.*, **6**, No. 2, 169–188. https://doi.org/10.1002/wsbm.1260

109. M. Selmi, W. C. Chiu, V. K. Chivukula, et al., *Int. J. Artif. Organs.*, **42**, No. 3, 113–124 (2019). https://doi.org/10.1177/0391398818806162

110. P. D. Morris, A. Narracott, H. von Tengg-Kobligk, et al., *Heart*, **102**, No. 1, 18–28 (2016). https://doi.org/10.1136/heartjnl-2015-308044

111. R. A. Gray and P. Pathmanathan, *J. Cardiovasc. Transl. Res.*, **11**, 80–88 (2018). https://doi.org/10.1007/s12265-018-9792-2

112. C. A. Taylor, T. A. Fonte, and J. K. Min, *J. Am. Coll. Cardiol.*, **61**, No. 22, 2233–2241 (2013). https://doi.org/10.1016/j.jacc.2012.11.083

113. R. Sadeghi, S. Khodaei, J. Ganame, and Z. Keshavarz-Motamed, *Sci. Rep.*, **10**, 9048 (2020). https://doi.org/10.1038/s41598-020-65576-y

114. V. A. Tkachuk, ed., *Clinical Biochemistry* [in Russian], GEOTAR-MED, Moscow (2004).

115. N. S. Key, M. Makris, and D. Lillicrap, eds., *Practical Hemostasis and Thrombosis. 3rd ed.*, Wiley–Blackwell, Hoboken (2017).

116. M. V. Samsonov, A. Y. Khapchaev, A. V. Vorotnikov, et al., *Oxid. Med. Cell. Longev.*, **2017**, 1625130 (2017). https://doi.org/10.1155/2017/1625130

117. L. Teuwen, V. Geldhof, A. Pasut, et al., *Nat. Rev. Immunol.*, **20**, No. 7, 389–391 (2020). https://doi.org/10.1038/s41577-020-0343-0

118. Z. Varga, A. J. Flammer, P. Steiger, et al., *Lancet*, **395**, No. 10234, 1417–1418 (2020). https://doi.org/10.1016/S0140-6736(20)30937-5

119. A. S. Rukhlenko, "Mathematical modeling of thrombosis processes in intensive blood flows," Ph. D. Thesis" [in Russian], Moscow Inst. Phys. Technol., Dolgoprudny (2013).

120. D. Bluestein, L. Niu, R. T. Schoephoerster, M. K. Dewanjee, *Ann. Biomed. Eng.*, **25**, 344–356 (1997). https://doi.org/10.1007/BF02648048

121. Y. Roka-Moiia, R. Walk, D. E. Palomares, et al., *Thromb. Haemost.*, **120**, No. 5, 776–792 (2020). https://doi.org/10.1055/s-0040-1709524

122. Y. N. Avtaeva, I. S. Mel'nikov, and Z. A. Gabbasov, *Bull. Exp. Biol. Med.*, **165**, No. 1, 157–160 (2018). https://doi.org/10.1007/s10517-018-4119-5

123. R. Radovancevic, N. Matijevic, A. W. Bracey, et al., *ASAIO J.*, **55**, No. 5, 459–464 (2009). https://doi.org/10.1097/MAT.0b013e3181b235af

124. S. R. Topper, M. A. Navitsky, R. B. Medvitz, et al., *Cardiovasc. Eng. Techn.*, **5**, 54–69 (2014). https://doi.org/10.1007/s13239-014-0174-x

125. K. Bourque, C. Cotter, C. Dague, et al., *ASAIO J.*, **62**, No. 4, 375–383 (2016). https://doi.org/10.1097/MAT.0000000000000388

126. S. Sukavaneshvar, *Adv. Drug Deliv. Rev.*, **112**, 24–34 (2017). https://doi.org/10.1016/j.addr.2016.07.009

127. W. Huberts, S. G. Heinen, N. Zonnebeld, et al., *J. Comput. Sci.*, **24**, 68–84 (2018). https://doi.org/10.1016/j.jocs.2017.07.006

128. P. Hariharan, G. A. D'Souza, M. Horner, et al., *PLOS ONE*, **12**, No. 6, e0178749 (2017). https://doi.org/10.1371/journal.pone.0178749

129. L. Goubergrits and K. Affeld, *Artif. Organs*, **28**, No. 5, 499–507 (2004). https://doi.org/10.1111/j.1525 1594.2004.07265.x

130. H. Yu, S. Engel, G. Janiga, D. Thévenin, *Artif. Organs*, **41**, No. 7, 603–621 (2017). https://doi.org/10.1111/aor.12871

131. J. D. Hellums, *Ann. Biomed. Eng.*, **22**, 445–455 (1994). https://doi.org/10.1007/BF02367081

132. H. Lee, G. Kim, C. Lim, et al., *Biomicrofluidics*, **10**, No. 6, 064118 (2016). https://doi.org/10.1063/1.4972077

133. H. C. Hemker, R. Al Dieri, S. Béguin, *Front. Med.*, **6**, 254 (2019). https://doi.org/10.3389/fmed.2019.00254

134. K. G. Guria, A. R. Gagarina, and G. T. Guria, *J. Theor. Biol.*, **304**, 27–38 (2012). https://doi.org/10.1016/j.jtbi.2012.03.031

135. D. P. Faxon, *Nat. Clin. Pract. Cardiovasc. Med.*, **2**, 22–28 (2005). https://doi.org/10.1038/ncpcardio0065

136. A. Meretoja, M. Keshtkaran, J. L. Saver, et al., *Stroke*, **45**, No. 4, 1053–1058 (2014). https://doi.org/10.1161/STROKEAHA.113.002910

137. S. G. Uzlova, K. G. Guria, A. A. Shevelev, et al., *Bull. A. N. Bakulev Nats. Tsentr Serd.-Sosud. Zabolev.*, **9**, No. 6, 55–64 (2008).

138. S. G. Uzlova, K. G. Guria, and G. T. Guria, *Philos. Trans. Roy. Soc. A*, **366**, No. 1880, 3649–3661 (2008). https://doi.org/10.1098/rsta.2008.0109

139. D. A. Ivlev, Sh. N. Shirinli, S. G. Uzlova, and K. G. Guria, *Biophysics*, **63**, No. 4, 637–643 (2018). https://doi.org/10.1134/S0006350918040085

140. C. D. Gerardo, E. Cretu, and R. Rohling, *Microsyst. Nanoeng.*, **4**, 19 (2018). https://doi.org/10.1038/s41378-018-0022-5

141. S. Merouche, L. Allard, and E. Montagnon, et al., *IEEE Trans. Ultrason. Ferroelectr. Freq. Control.*, **63**, No. 1, 35–46 (2015). https://doi.org/10.1109/TUFFC.2015.2499084

142. N. V. Rybalko, O. I. Vinogradov, and A. N. Kuznetsov, *Nevrol. Zh.*, **20**, No. 5, 14–18 (2015).

143. T. Knebel and J. J. Neumiller, *Clin. Diab.*, **37**, No. 1, 94–95 (2019). https://doi.org/10.2337/cd18-0067

144. K. Hasan, K. Biswas, K. Ahmed, et al., *J. Netw. Comp. Appl.*, **143**, 178–198 (2019). https://doi.org/10.1016/j.jnca.2019.06.016?

145. L. Antiga, B. Ene-Iordache, and A. Remuzzi, *IEEE Trans. Med. Imaging*, **22**, No. 5, 674–684 (2003). https://doi.org/10.1109/TMI.2003.812261

146. W. Lorensen and H. Cline, *ACM SIGGRAPH*, **21**, No. 4, 163–169 (1987). https://doi.org/10.1145/37402.37422

147. M. Bozzetto, B. Ene-Iordache, and A. Remuzzi, *Ann. Biomed. Eng.*, **44**, No. 8, 2388–2401 (2016). https://doi.org/10.1007/s10439-015-1525-y

148. L. Antiga, M. Piccinelli, L. Botti, et al., *Med. Biol. Eng. Comput.*, **46**, No. 11, 1097–1112 (2008). doi10.1007/s11517-008-0420-1

149. A. Wittek, N. Grosland, G. Joldes, et al., *Ann. Biomed. Eng.*, **44**, No. 1, 3–15 (2016). https://doi.org/10.1007/s10439-015-1469-2

150. https://cfmesh.com/

151. T. Pedley, *The Fluid Mechanics of Large Blood Vessels*, Cambridge Univ. Press, Cambridge (1980).

152. C. J. Nassau, T. J. Wray, and R. K. Agarwal, in: *FEDSM 2015, July 26–31, 2015, Seoul, South Korea*, p. V002T26A002. https://doi.org/10.1115/AJKFluids2015-26131

153. A. Ribes and C. Caremoli, in: *COMPSAC 2007, July 24–27, 2007, Beijing, China*, pp. 553–564. https://doi.org/10.1109/COMPSAC.2007.185

154. C. Patankar, *Numerical Heat Transfer and Fluid Flow*, Hemisphere, New York (1980).

155. R. Issa, *J. Comp. Phys.*, **62**, No. 1, 40–65 (1986). https://doi.org/10.1016/0021-9991(86)90099-9

156. M. Bozzetto, P. Brambilla, S. Rota, et al., *Int. J. Artif. Organs*, **41**, No. 11, 714–722 (2018). https://doi.org/10.1177/0391398818784207

157. F. Menter and T. Esch, in: *COBEM 2001, November 26–30, 2001, Uberlândia, Brazil*, pp. 1–11.

158. H. Jasak, in: *47th AIAA Aerospace Sciences Meeting, January 5–8, 2009, Orlando, USA*, pp. 1–10. https://doi.org/10.2514/6.2009-341

159. H. Jasak, *Inter. J. Nav. Archit. Oc. Engin.*, **1**, No. 2, 89–94 (2009). https://doi.org/10.2478/IJNAOE 2013 0011

160. J. Ahrens, B. Geveci, and C. Law, in: C. D. Hansen and C. R. Johnson, eds., *The Visualization Handbook*, Butterworth–Heinemann, Burlington, MA, pp. 717–731 (2005). https://doi.org/10.1016/B978 012387582 2/50038-1

161. T. Kenner, *Basic. Res. Cardiol.*, **84**, No. 2, 111–124 (1989). https://doi.org/10.1007/BF01907921

162. C. A. Taylor and C. A. Figueroa, *Annu. Rev. Biomed. Eng.*, **11**, 109–134 (2009). https://doi.org/10.1146/annurev.bioeng.10.061807.160521

163. D. Lesage, E. D. Angelini, I. Bloch, and G. Funka-Lea, *Med. Image Anal.*, **13**, No. 6, 819–845 (2009). https://doi.org/10.1016/j.media.2009.07.011

164. S. Moccia, E. De Momi, S. El Hadji, and L. S. Mattos, *Comput. Meth. Prog. Bio.*, **58**, 71–91 (2018). https://doi.org/10.1016/j.cmpb.2018.02.001

165. F. Zhao, Y. Chen, Y. Hou, and X. He, *Multimedia Systems*, **25**, No. 2, 109–118 (2019). https://doi.org/10.1007/s00530-017-0580-7

166. A. Updegrove, N. Wilson, J. Merkow, et al., *Ann. Biomed. Eng.*, **45**, 525–541 (2016). https://doi.org/10.1007/s10439-016-1762-8

167. S. Lippok, T. Obser, J. P. Müller, et al., *Biophys. J.*, **105**, No. 5, 1208–1216 (2013). https://doi.org/a10.1016/j.bpj.2013.07.037